On the simulation-based quantification of energy dissipation in rockfall protection structures: Case of an articulated wall modelled with the NSCD method

Stéphane Lambert, Ritesh Gupta, Franck Bourrier, Vincent Acary

To cite this version:

Stéphane Lambert, Ritesh Gupta, Franck Bourrier, Vincent Acary. On the simulation-based quantification of energy dissipation in rockfall protection structures: Case of an articulated wall modelled with the NSCD method. Rock Mechanics and Rock Engineering, In press, pp.1-47. hal-04767017v3

HAL Id: hal-04767017

https://hal.science/hal-04767017v3

Submitted on 5 Nov 2024

HAL is a multi-disciplinary open access archive for the deposit and dissemination of scientific research documents, whether they are published or not. The documents may come from teaching and research institutions in France or abroad, or from public or private research centers.

L'archive ouverte pluridisciplinaire **HAL**, est destinée au dépôt et à la diffusion de documents scientifiques de niveau recherche, publiés ou non, émanant des établissements d'enseignement et de recherche français ou étrangers, des laboratoires publics ou privés.

Copyright

Highlights

- A rigorous scheme is proposed for computing energy dissipation by both friction and plastic strain in the Non-smooth contact dynamics (NSCD) framework.
- The structure dissipative capacities computed from simulation results are addressed in terms of the ratio $R_{f/p}$ between the energy that is dissipated by friction to that dissipated by plastic strain.
- The structure dissipative capacities assessed from simulation results, including the ratio $R_{f/p}$, reveal sensitive to the way how the model parameters were calibrated and, to a larger extent, to the impact conditions.
- The ratio $R_{f/p}$ appears relevant for describing the whole structure response over a wide range of realistic impact conditions.

On the simulation-based quantification of energy dissipation in rockfall protection structures: Case of an articulated wall modelled with the NSCD method

Stéphane Lambert[1*], Ritesh Gupta[1], Franck Bourrier[1,2], Vincent Acary[2]

[1*]Univ. Grenoble Alpes, INRAE, CNRS, IRD, Grenoble INP, IGE
Grenoble, 38000, France.
[2]Univ. Grenoble Alpes, Inria, CNRS, Grenoble INP, Institute of
Engineering, LJK Grenoble, 38000, France.

Abstract

This article focuses on the key issue of energy dissipation in passive rockfall protection structures when exposed to impact by a rock block. As an application case, a structure consisting of a wall made of interconnected concrete blocks is considered. A Non-Smooth Contact Dynamics (NSCD) model of this structure was previously developed and calibrated with respect to the spatio-temporal impact response obtained from real-scale impact experiments. The NSCD model accounts for energy dissipation due to friction between the system bodies and to plastic strain at contacts. The energy dissipation computation method is detailed and its exactness is demonstrated considering two impact cases. The evolution with time of energy dissipation by each dissipative mechanism provides insights into the global structure response with time in terms of displacement and contact force amplitude. The influence of the model parameters on the contribution of these two dissipative mechanisms is evaluated. A ratio between energy dissipation by friction to energy dissipation by plastic strain is proposed as a criterion for structural response evaluation. The variability in energy dissipation varying the impact conditions is addressed. In the end, this study reveals the benefits derived from a precise quantification of energy dissipation in passive rockfall protection structures. Beyond the considered application case, such an approach focusing on energy dissipation opens up promising prospects for improving the design of all passive rockfall mitigation structures.

Keywords: rockfall, impact, NSCD model, energy dissipation

1 Introduction

Passive rockfall protection structures such as flexible barriers, galleries, walls and embankments are often built on slopes to intercept or deviate rock blocks with kinetic energies sometimes exceeding 10 MJ (Volkwein et al, 2011). These protection structures are thus designed to withstand the severe localised dynamic loading they are exposed to during their normal operation. During impact, the structure experiences displacement and damage, with an amplitude that depends on the reduction in rock block kinetic energy over the impact duration. The kinetic energy lost by the rock block is progressively dissipated in the structure and, to a lesser extent, transferred to its foundation such as anchors, if any, and then to the surrounding environment which most often consists of ground or bedrock. The structure's mechanical response and efficiency with respect to its purpose is highly dependent on its capacity to transfer and dissipate energy.

Energy dissipation in structures exposed to impacts by rock blocks is more and more addressed dealing with flexible barriers (Duan et al, 2023; Dhankal et al, 2012; Xu et al, 2018; Liu et al, 2018; Yu et al, 2019; Castanon-Jano et al, 2019; Di Giacinto et al, 2020; Previtali et al, 2021), embankments and walls (Ronco et al, 2009; Furet et al, 2022; Marchelli and Deangeli, 2022), steel posts (Zhao et al, 2021; Ng et al, 2023), cushion materials and energy dissipators (Previtali et al, 2021; Yan et al, 2022; Liang et al, 2022; Yang et al, 2024). Dissipation in rockfall protection structures mainly results from plastic damage (or plastic strain) of the structure materials and components and from friction within materials or at the interface between the structure components. Other dissipative mechanisms, such as thermal dissipation, are generally negligible or considered as such. The prevailing dissipative mechanism depends on the structure type, its constitutive materials and design as well as on the incident rock block kinetic energy. The vast majority of research works addressing energy dissipation are based on simulation results, making use of commercially available or in-house codes which are based on finite element, finite difference or discrete element methods (FEM, FDM and DEM resp.). All these models rely on simplifications and assumptions in particular concerning the realism of the structure description and the considered constitutive laws. In the best case, the model parameters are calibrated and/or validated against results from experiments on real-scale structures.

By comparison with experiments, numerical simulations give much easier access to the various data necessary for computing energy terms, and in particular the dissipative terms. Nevertheless, in all but a few research such as Ng et al (2023), the soundness of the energy terms quantification is debatable for various reasons. In many cases, not all the energy terms were taken into account or mentioned. This is the case for elastic strain energy and for the variation in potential energy, even when large mass components experience significant displacement along the vertical axis. Sometimes, the absence of the term is because some commercially available simulation tools do not provide the user with all necessary data (e.g. Furet et al (2022); Yang et al (2024)).

Most often, very limited details are provided concerning the way the various energy terms were computed while the energy balance of the numerical method employed can play an important role. Explicit schemes can artificially inject energy into the system if the time discretisation is too coarse. This problem is often avoided for computational stability reasons by adding viscous dissipation to the system which is not justified by the physics of the phenomenon. Conversely, purely implicit schemes, such as the Euler backward scheme, dissipate a lot of energy numerically, which stabilises the numerical simulation. Even though dissipation associated with these numerical artefacts is easy to compute, the provided results may not be conducive to the safety of protective structures. In the end, compliance with the fundamental principle of energy conservation in the system is rarely supported by evidences while it is a prerequisite for giving confidence in the simulation results. In many cases, this compliance is debatable or it can't be checked a posteriori, as for example in Di Giacinto et al (2020).

This article proposes a detailed and rigorous investigation of energy dissipation in a particular and complex type of rockfall protection structure made from piled-up and interconnected concrete blocks. This rockfall protection wall is first described. The structure model previously developed under the NSCD framework and implemented in the SICONOS software is briefly presented. The new method by which energy dissipation by friction and plastic strain is calculated from the simulation results is then detailed, revealing a particular time integration scheme that meets energy conservation requirements. The investigation that follows is conducted under the hypothesis that the concrete block model and the dissipative mechanisms are appropriate with respect to the addressed topic. A detailed analysis of energy balance computed based on the simulation of the two impact tests performed on the real structures is conducted to reveal the interest in considering the dissipative mechanisms for describing the whole structure response with time. The influence of the way the model parameters are calibrated and of the impact conditions on the respective contribution of friction and plastic strain in energy dissipation is then investigated. The ratio between the amount of energy dissipated by friction to that dissipated by plastic strain is employed for describing the structure response and for characterising its dissipative capacities. Combined with the energy transferred to the structure, this ratio appears relevant for investigating the structure dissipative capacities when considering a large set of realistic impact conditions.

2 Considered rockfall protection structure and its model

This research focuses on a specific type of rockfall protection structure made of concrete blocks interconnected one to another to form articulated walls. This type of massive rockfall protection structure has the advantage of having a reduced footprint, similarly to other structures (Lambert et al, 2019; Korini et al, 2021). The development of this structure type involved real-scale impact experiments together with numerical modelling.

2.1 Structure description

The structure consists of concrete blocks, 1850kg in mass each, that are piled up in staggered rows (Fig. 1). Superimposed concrete blocks are traversed along the vertical axis by connectors consisting of assemblies of metallic tubes and cables whose aim is to ensure mechanical continuity of the wall. The concrete block shape favours relative rotation between adjoining blocks in the same horizontal row. The wall deformation capacity is further increased by the space left between tubes and concrete blocks, on one side, and between adjoining concrete blocks on the same horizontal row on the other. This innovative technology offers the possibility to build massive vertical walls, with reduced footprint, high deformability and versatility. For example, different geometric arrangements of the concrete blocks along the longitudinal axis can be adopted such as the zig-zag pattern considered in this study or a linear wall, with or without partition walls (Furet et al, 2022). Such structures are intended to serve as passive protection against gravity-driven natural hazards, and in particular rockfall. A key feature of this structure type lies in the fact that the interconnections between the concrete blocks improve the structure stability preventing excessive concrete block displacements nearby the impact location.

Depending on the kinetic energy of the rockfall to intercept, a boulder impact on such an articulated wall may induce concrete crushing and fracture, basal sliding, wall tilting and relative displacement between superimposed concrete blocks with each an amplitude that decreases with the distance to the impact location (see Furet et al (2022); Gupta et al (2023, 2024)). The structure is described with more details in Furet et al (2022).

2.2 The NSCD structure model

The structure was modelled using the SICONOS software package (Acary and Perignon, 2007; Acary et al, 2019) which is based on the Non-Smooth Contact Dynamics (NSCD) approach (Jean and Moreau, 1987; Jean, 1999; Dubois et al, 2018). The choice of NSCD modelling was preferred over FEM, FDM and DEM for computation time reasons. With NSCD, one simulation with a personal computer typically lasted 20 minutes, compared to 10 hours with the finite difference model proposed by Furet et al (2022). Running thousands of simulations for example in view of investigating the structure response varying the impact conditions thus becomes affordable.

The layout of the wall model is presented in Figure 2 comprising of modelled components for blocks, connectors and projectile. The mechanical and geometrical properties of most of the components are directly taken from the real structure. However, five model parameters cannot be directly assigned. Three parameters concerned the contact mechanics, namely the restitution coefficient, e, and two friction coefficients, μ_{cc} and μ_{cs}, for concrete-concrete interfaces and concrete-supporting surface interface respectively. These three parameters are intrinsic to the modelling approach and are not easy to measure precisely under dynamic conditions. The two other parameters have been integrated into the model to traduce specific features of the structures that are of paramount importance for its functional efficacy. The first parameter, v_p, represents the relative looseness in the cable connecting the concrete blocks and the second one, d_z, defines the position of the virtual disk that enables the contact between the blocks and the tubes. The need for calibration of these two parameters resulted from a large value variability and from difficulty in determining a relevant and precise value from measurements. More details concerning the way the structure was represented are provided in Gupta et al (2023).

The main lines of the computation method are described in Appendix A and an exhaustive description is given in Acary and Collins-Craft (2024), in the case of linear elasto-dynamics. The computation method is based on the Frémond's approach that consists of using the post-impact velocity instead of the average velocity of the pre-impact and post-impact velocities (Frémond, 2017; Frémond, 2002). This method differs from the more classical approach which was in particular used by the authors in their previous work (Gupta et al, 2023). It was preferred in this study because preliminary simulations emphasised that the classical approach resulted in slight energy balance discrepancies in the rare case of a sliding velocity reversal during impact.

2.3 Model calibration

The calibration of the five model parameters made use of measures collected during two impact tests on real-scale structures, 14m long and 3.2m high. These impact tests involved a projectile 1.1m in size with kinetic energy at the impact of 520 and 1020 kJ (Furet et al, 2022). The considered measurements were the displacement at four points in the structure, as illustrated in Figure 2, and at three times instants, *i.e.*, for a total of 24 measures. Calibrating the model parameters against this set of data thus allows accounting for the whole structure displacement with time and space, under two different loading conditions.

The calibration was conducted based on a complex and innovative approach quantitatively minimising the model prediction error in terms of wall displacement with time and space. This approach relied on the Bayesian inference statistical learning method, accompanied by the meta-modelling techniques. It is described in Gupta et al (2023).

This approach resulted in the parameter values presented in the first row of Table 1 which define the reference model used in the following. These values slightly differ from that in Gupta et al (2023) due to the improvement in the computation scheme presented in section 2.2 and Appendix A. The set of model parameters presented in the other rows of this table will be used in section 4.

The significant effort made for calibrating the five model parameters based on 24 data describing the spatio-temporal response of the structure is considered to give confidence in the reference model's predictive capacity. By contrast, it is thought that a calibration based on a smaller data set would have resulted in a less efficient model for predicting the whole structure displacement when varying the impact conditions for example.

3 Energy dissipation computation

This section first introduces the method established for computing energy dissipation from the model simulation results. This method is then applied to two cases for its validation.

3.1 Energy terms computation

This section presents the way energy dissipation terms were computed. In the equations below, the subscripts N, T and k respectively refer to the normal component, the tangential component and the computation step. The superscripts α, $+$ and $-$ respectively refer to the considered contact point, and the post- and pre-impact situations.

The discrete kinetic energy, K, is defined as:

$$K_{k+1} = \frac{1}{2} v_{k+1}^{\top} M v_{k+1}, \tag{1}$$

with v the generalised velocity vector which contains the centre of mass velocities and the angular velocities expressed in the body frame and M the mass matrix.

The variation of energy due to the work of forces, ΔP, is defined as

$$\Delta_k^{k+1} P = -h v_{k+1/2} F_{k+1/2}. \tag{2}$$

with h the time step and F the force vector that collects the externally applied forces and the gyroscopic effects. The notation $\Delta_k^{k+1} P$ is used to outline that the work of forces over a time interval is equal to the variation of the potential energy if the gyroscopic forces vanish.

The work associated with the normal component of a contact impulse is given by:

$$w_{\mathrm{N}}^{\alpha} = \frac{1}{2}(u_{\mathrm{N}}^{\alpha,+} + u_{\mathrm{N}}^{\alpha,-}) p_{\mathrm{N}}^{\alpha} = \frac{1}{2}(1 - e^{\alpha}) u_{\mathrm{N}}^{\alpha,-} p_{\mathrm{N}}^{\alpha} \leq 0 \tag{3}$$

since $u_{\mathrm{N}}^{\alpha,-} \leq 0$ and $p_{\mathrm{N}}^{\alpha} \geq 0$, with u the local relative velocity, p the contact impulse and e the restitution coefficient

The work associated with the tangential component of a contact impulse is computed as:

$$w_{\mathrm{T}}^{\alpha} = \frac{1}{2}(u_{\mathrm{T}}^{\alpha,+} + u_{\mathrm{T}}^{\alpha,-}) p_{\mathrm{T}}^{\alpha} = -\mu^{\alpha} \|\bar{u}_{\mathrm{T}}\| p_{\mathrm{N}}^{\alpha} \leq 0. \tag{4}$$

with μ the friction coefficient.

The discrete work of all contact impulses is given by:

$$W_{k+1} = \sum_{\alpha \in I} u^{\alpha}_{k+1/2} p^{\alpha}_{k+1}, \tag{5}$$

that be decomposed in its normal

$$W_{\mathrm{N},k+1} = \sum_{\alpha \in I} u^{\alpha}_{\mathrm{N},k+1/2} p^{\alpha}_{\mathrm{N},k+1} = \sum_{\alpha \in I} \frac{1}{2}(1 - e^{\alpha}) u^{\alpha}_{\mathrm{N},k} p^{\alpha}_{\mathrm{N},k} \tag{6}$$

and tangent parts

$$W_{\mathrm{T},k+1} = \sum_{\alpha \in I} u^{\alpha}_{\mathrm{T},k+1/2} p^{\alpha}_{\mathrm{T},k+1} = \sum_{\alpha \in I} -\frac{1}{2} \mu^{\alpha} \| u^{\alpha}_{\mathrm{T},k+1} + u^{\alpha,-}_{\mathrm{T},k+1} \| p^{\alpha}_{\mathrm{N},k}. \tag{7}$$

It is shown in Acary and Collins-Craft (2024), in the case of linear elasto-dynamics, that the discrete work of contact forces is non-positive and the following discrete energy balance is satisfied

$$\Delta K_k^{k+1} + \Delta_k^{k+1} P = W_{k+1}, \text{ with } W_{k+1} \leq 0. \tag{8}$$

where $\Delta K_k^{k+1} = K_{k+1} - K_k$. Numerical evidence shows this relation is also satisfied in the case of rigid bodies under gravity.

The energy dissipation due to the work of the tangential components of contact impulses ($W_{\mathrm{T},k+1}$) is directly related to frictional processes. Consequently, the cumulative energy dissipated by friction is :

$$D_f = -\sum_{k=0}^{N} W_{\mathrm{T},k+1} \geq 0. \tag{9}$$

The remaining part of the work of the contact impulses, that is the contribution of the normal components of contact impulses ($W_{\mathrm{N},k+1}$), is associated with energy dissipation (D_p) due to plastic strain associated with concrete blocks damage, in particular in the vicinity of the impact point. D_p is defined as

$$D_p = -\sum_{k=0}^{N} W_{\mathrm{N},k+1} \geq 0, \tag{10}$$

Over the whole time interval of simulation, we have the energy balance

$$\Delta(K + P) = -(D_p + D_f). \tag{11}$$

In other words, the total energy of the system decreased over time by the amount of dissipation at contacts by friction and plastic strain.

3.2 Application to the reference impact cases

The previously described method was employed for computing energy dissipation in the case of the two impact tests conducted on the real-scale structures (Furet et al, 2022). The considered simulation time step was 0.25 milliseconds and the simulated impact duration was 1 second (see the video of a simulation with this link).

Figure 3 shows for the two impact cases the evolution with time of the kinetic energy and variation in potential energy of all the concrete blocks (K_{wall} and ΔP_{wall}, resp.), the sum of the variation in potential energy and the kinetic energy of the projectile ($\Delta P_{proj} + K_{proj}$). K_{proj} comprises of the rotational and translational kinetic energies. The initial value of the former component is nil for these two impacts but will be varied in the following. This Figure also shows the cumulative energy dissipated by friction at all interfaces (D_f) and by plastic strain (D_p). The sum of all these energy terms is also plotted (Σ). All these quantities are normalised by the projectile kinetic energy at impact, $K_{proj}(t_0)$.

It is assumed that, at the projectile-wall contact, energy dissipation only occurs in the impacted concrete block, which is consistent with the absence of projectile damage observed after the experiments. In these plots, kinetic energy accounts for both translational and rotational energies. For presentation clarity purposes, the interaction of the projectile with the ground after it bounced away from the wall is not simulated.

The first observation from Figure 3 is that the sum of all these quantities remained constant, with a nearly nil variation over time. This shows that the energy balance equation (Eq. 8) is respected and demonstrates the soundness of the computation scheme.

The two impact cases exhibit similar trends. The projectile total energy, ΔP_{proj} + K_{proj}, sharply decreased at the very impact beginning, as a consequence of its translational velocity reduction associated with the impact with the wall. Just after the projectile lost contact with the wall, its velocity was small, with values of 10.7% for the incident velocity for the 520kJ impact, and 5.6% for the 1020kJ one. The variation in concrete blocks' potential energy, ΔP_{wall}, remained small with a maximum value attained at 0.15 second approximately (amounting to less than 4% the impact energy), suggesting a limited upward displacement of the concrete blocks. By contrast, the concrete block kinetic energy, K_{wall}, experienced a high variation over the first tenths of milliseconds , with a maximum amounting more than 20% the impact energy in both cases. It took more than 0.5 seconds before the wall kinetic energy was close to zero, with a slightly higher duration for the 1020kJ impact.

Dissipation by plastic strain, D_p, mainly occurred at the very beginning of the impact. Nearly 90% of the total dissipation by plastic strain was reached less than 0.1 seconds after the projectile touched the wall. Dissipation by plastic strain lasted longer for the 1020kJ impact case (more than 0.4 seconds). In contrast, the cumulative energy dissipation by friction, D_f, increased more progressively and stopped increasing after 0.55 seconds approximately.

For both impact cases, the dominating dissipative mechanism over the whole impact duration reveal to be plastic strain. In the end, energy dissipation by plastic strain amounted to approximately 65% of the incident projectile kinetic energy for both the 520kJ and the 1020kJ impact. The remaining was dissipated by friction.

These curves and the derived trends reflect the whole structure response with time and space. Energy dissipation by plastic strain traduces the amplitude of the normal impulse between system components. Energy dissipation by friction traduces the amplitude of the relative displacement in the tangential direction between system components, and mainly the concrete blocks and the supporting surface. Both dissipative mechanisms initiate nearby the impact location and progressively concern components at a further distance, depending on the amplitude of contact force and displacement. Most of the dissipation by plastic strain occurs in typically 0.2 seconds indicating a rapid decrease in contact force amplitude between the blocks throughout the wall. At 0.2 seconds , the wall still moves and dissipation by friction lasts until sliding at its base stops (typically around 0.6 seconds).

3.3 Dissipation-based descriptor of the structure response

This description clearly shows that quantities associated with energy dissipation in the system describe the whole structure response, with time and space, in a rather clear and synthetic manner. The respective contributions of the dissipative mechanisms over time are highlighted.

The predominance of plastic strain in energy dissipation after the wall is at rest (i.e. after impact) is evidenced by the ratio between the cumulative values of the energy dissipated by friction, D_f, and the energy dissipated by plastic strain, D_p, referred to as $R_{f/p}$. This dissipation ratio takes values of about 0.56 and 0.55 for the

520kJ- and 1020kJ-impacts respectively indicating that dissipation by plastic damage dominates. A similar general conclusion was obtained by Furet et al (2022) based on simulations with the finite volume formulation code FLAC3D. The model accounted for the structure components and geometry in a very realistic way. The constitutive laws accounted for plasticity, in particular for modelling damage to concrete blocks. The authors concluded that plastic strain was the dominating dissipative mechanism, with an average $R_{f/p}$ value of approximately 0.5 considering the same two tests. Nevertheless, it was not possible for Furet et al (2022) to access all quantities associated with energy, resulting in a 26% difference between the incident projectile kinetic energy and the sum of all computed terms.

To some extent, the value of the $R_{f/p}$ ratio reflects the response of the structure, in terms of displacement and contact force over the whole impact duration and whole structure. A high ratio value indicates that the whole structure impact response with time is characterised by significant block displacements, resulting in high dissipation by friction and, vice versa, a small $R_{f/p}$ value reveals that the structure impact response is characterised by large contact forces resulting in damage to the blocks. The $R_{f/p}$ ratio thus appears a relevant and synthetic descriptor of the whole structure response and, for this reason, it will be considered in the following for discussing the variability in the response of the articulated wall addressed in sections 4 and 5.

4 Sensitivity of energy dissipation to model parameters

Parameters calibration is a crucial stage in the development of a numerical model, which can be based on data from experiments on real structures. In this section, we assess the extent to which the number of experimental data used for this calibration can influence the quality of the model's predictions with regard to energy dissipation.

4.1 Models parameters definition

The parameters of the reference model which are presented in the first row of Table 1 were calibrated using a fine-tuned approach considering 24 measurements obtained from impact experiments on real-scale structures (Section 2.3). More precisely, this set of best-fit parameters was defined so that the deviation of the model predictions with all these experimental data was minimised. Besides, results presented in Gupta et al (2023) evidenced that decreasing the number and variety of data used for calibrating the model parameters had a significant influence on the model accuracy in modelling the whole structure response with time. This clearly suggests that the strategy considered for calibrating the model parameters may have a significant influence on energy dissipation quantification by the model.

The dependence of energy dissipation quantification on the model parameters was addressed considering different sets of model parameters that were calibrated from the available experimental data set and following different calibration strategies with increasing complexity (Table 2). These strategies were in particular inspired by what is presented in the literature. The most simple strategy for calibrating a model consists of considering the displacement measured when the structure is at rest of one point in the structure. This point is generally located near the impact point. In our case, the experimental measurements at this location were globally not reliable or not available (Furet et al, 2022). For this reason, we considered the wall displacement after the 520kJ-test at the base, at the Top and at point D (see Fig. 2) which correspond to calibration strategies (CS) 1 to 3 in Table 2. The other strategies consist of considering displacement at different locations in the structure, different time instances (namely "Rest", "Init." and "max" as defined in Gupta et al (2023)) and different impact energies. These strategies were defined in a rather arbitrary manner.

Overall, strategies 1 to 9 consisted of calibrating the model parameters by comparing the model predictions with different selections of one to three data measured during the real-scale experiments. In other words, each of these nine models was calibrated to provide the best estimate for the displacement at the considered point, time instant and impact energy. This implicitly means that predictions at other points, time instants and energy are not expected to be good.

The calibration strategies presented in Table 2 globally give priority to data measured during the 520kJ-test as this kinetic energy is more in accordance with the kinetic energy to which this protection structure is intended. By contrast, the 1020kJ-test corresponds more to an extreme situation in terms of incident projectile kinetic energy, inducing severe damage to the wall. In principle, these energy levels may be respectively assimilated to service and limit energy levels (SEL and MEL) considered for flexible barriers (EOTA, 2018). Also, priority is given to calibration strategies considering measurements at rest, which is a frequent practice when calibrating models on a quantitative basis.

For each strategy, the calibration of the model parameters followed the same scheme as for the reference model, making use of the Bayesian inference accelerated with polynomial chaos expansion (PCE) based meta-models (section 2.3). The values presented in Table 1 confirm that the model parameters value vary significantly depending on the way the model was calibrated. For example, the maximum relative difference in parameter value with the reference model exceeds 50% (e.g., e equals 0.107 for CS8 vs 0.221 for the reference model).

The nine structure models, corresponding to these nine sets of calibrated parameters, were employed to simulate the structure response when exposed to impacts with energies of 520 and 1020kJ. The comparison between the results from the nine models is based on the $R_{f/p}$ ratio, as this ratio reflects the structure response via the relative contribution between the two dissipative mechanisms. More precisely, the relative difference in $R_{f/p}$ for a given model with that computed from simulations with the reference model is presented in Figure 4.

4.2 Comparison of the models predictions

By comparison with the reference case, twelve predictions of $R_{f/p}$ out of eighteen reveal rather good, with a difference less than 10% for one impact energy at least. This difference is less than 5% for six predictions. Models that were developed following calibration strategies CS4 and CS8 resulted in the best predictions among all nine models, with a difference of less than 5% for both impact energies. The worse predictions are provided by CS2, CS3 and CS5, with at least one prediction with a difference exceeding 15%.

The four models that were calibrated based on displacement at rest after the 520kJ-test only (CS1, CS2, CS3 and CS8) all underestimate $R_{f/p}$ for the 520kJ impact energy. All nine models underestimate $R_{f/p}$ for the 1020kJ impact case which is attributed to the set of data chosen for the nine strategies and in particular to the fact that these sets globally gave priority to data from the 520kJ impact test. A global trend is observed where a larger number of input data for the calibration results in better predictions. Nevertheless, the fact that differences less than 5% were obtained with the CS4 model, in which calibration considered one input data only, suggests this is not a strict rule.

Focusing on the calibration strategies resulting in the worst predictions, namely CS2 and CS5, Figure 5 reveals a significant difference with the reference model in terms of energy dissipation by friction and by plastic strain during the impact. For the 1020kJ-impact case, the models calibrated against CS2 and CS5 underestimate D_f by about 14% and 7% and consequently, both models overestimate D_p. For the 520kJ-impact case, D_f is overestimated by one model (CS5) and underestimated by the other (CS2), with a 10% deviation approximately in both cases. The opposite trend is observed focusing on D_p. Last but not least, the differences with the reference model in terms of both D_f and D_p clearly appear from the early stages of the wall response to impact, revealing a significant difference in terms of blocks displacement with time and space.

4.3 On the model parameters calibration

The results presented in the previous section evidenced that the way the model parameters are calibrated may have a significant influence on the accuracy of simulation-based estimation of the energy dissipative capacities of the wall. This is obviously due to the fact that the model parameters govern the overall dynamic response of the structure, in terms of displacement and load transfer with time and space, which has consequences on energy dissipation by both friction and plastic strain. The predictions of models calibrated against two or three data appeared surprisingly good, some showing a difference in $R_{f/p}$ value less than 5 % with the reference model. By contrast, the difference for models calibrated against one data was globally much higher, with some values exceeding 15 %.

The general trend where a higher number of data results in better predictions is not a rule, which suggests that for a model to be reliable, its parameters should be calibrated against a rich set of data, meaning a set conveying information reflecting the spatio-temporal structure impact response. For this structure, a data set consisting in two displacement measurements (at different locations, time or for different projectile kinetic energies) generally revealed sufficiently rich. It is thought that the number and type of data to be used for getting a rich data set is structure-dependent meaning that this conclusion should be considered with caution when dealing with other structure types. Besides, getting a rich data set from real-scale experiments requires that the experimental set-up was designed to get many data, as for example the displacement at different locations or at different time instances.

Paying particular attention to the reliability of the model predictions is even more necessary when energy dissipation quantification constitutes the basis of a design method. This is for example the case with the analytical method proposed by Marchelli and Deangeli (2022) to design rockfall protection embankments which is based on the simulation-based estimation that 85 % of the incident projectile kinetic energy is dissipated by plastic strain in the embankment.

It is important to remind that, as with any model, the numerical model of this structure relies on different simplifications and assumptions which may have consequences on the model predictions in terms of energy dissipation. The proposed NSCD model accounts for concrete block damage in a simple way, with the advantage of a reduced computation time. It has been calibrated so that displacements in time and space can be predicted with good accuracy. Using this model for computing energy dissipation implicitly lies on the hypothesis that all physical processes involved in energy dissipation are accounted for. Demonstrating this rigorously is out of reach, due to both experimental and numerical constraints and limitations. As for the former, this demonstration would require additional measurements that are difficult, if not impossible, to make (impact strength of highly reinforced blocks, relative displacement between blocks...). As for the latter, it would require substantial increase in the model complexity that would lead to excessively long computations. This research is thus based on two working hypotheses which concern the use of a simple model for the blocks and the dissipative mechanisms.

5 Energy dissipative capacities over a large range of impact conditions

On-site rockfall protection structures are exposed to a wide variety in impact conditions during their normal operation. Up to now, the induced variability in response of rockfall protection structures has mainly been addressed focusing on their deformation or deflection, load transmission and failure (Breugnot et al, 2016; Mentani et al, 2016; Bourrier et al, 2016; Toe et al, 2018; Previtali et al, 2021; Lambert et al, 2021;

Douthe et al, 2022; Qi et al, 2022; Maheshwari et al, 2024). It is here proposed to address the variability in structure response in terms of energy dissipation.

5.1 Impact conditions definition

In the previous section, the structure response was addressed considering two impacts in the centre of a 14m long wall, by a projectile with a normal-to-the-wall incident trajectory. These test conditions are consistent with current practices for rockfall protection structures testing, such that prescribed for flexible barriers (EOTA, 2018), but are not representative of field conditions where impacts may occur under very different conditions. These impact tests constitute conformance tests that may not be representative of the on-site structure response. For this reason, and in a similar way as previously done for flexible barriers (Mentani et al, 2016; Toe et al, 2018; Previtali et al, 2023), the investigation of the zig-zag wall response was expanded varying the impact point location, the translational and rotational velocities of the incident projectile, the deviation of its trajectory with respect to the horizontal axis and with respect to the normal to the wall longitudinal axis. Realistic ranges have been considered for these parameters (Table 3). The range for the impact point location along the vertical axis, z, considered a minimum value equal to the projectile radius at the toe of the wall and a free-board equal to the projectile diameter at its top, in accordance with some design practices (Lambert and Bourrier, 2013). The impact point location along the horizontal axis, y, was varied from the wall centre to a distance of 3.53m aside, in accordance with the length of the zig-zag pattern of this wall. The range for the translational velocity, v, corresponds to translational kinetic energies from 130 to 810kJ. The maximum value is about 20% less than the wall nominal capacity (considered to be 1020kJ based on the experiments) to limit severe damage to concrete blocks. The considered ranges for the projectile rotational velocity, Ω, inclination and deviation were derived from the literature (Bourrier et al, 2012; Toe et al, 2018; Noël et al, 2023). The same projectile as in the previous section was considered. The wall length was increased to 28.2m to limit boundary effects while keeping the computation time reasonable. The structure response description proposed hereafter is thus relevant whatever the impact point location and providing that the wall extremities experience very limited displacement. This condition can be insured on-site with ground abutments or shrouds at the wall extremities.

These impact conditions were also considered by the authors for conducting an inverse analysis of the wall response to serve in operational contexts (Gupta et al, 2024).

A Latin hypercube sampling method (Lataniotis et al, 2015) was employed to generate 300 sets of 6 input parameters from the ranges presented in Table 3 for running simulations with the reference NSCD model of the wall.

5.2 Influence of the impact conditions on the structure response

The variability in structure response varying the impact conditions is illustrated from the 300 simulations results in Figure 6 focusing on the post-impact displacement at the top of the wall. This figure shows the location of the extremity of the structure's vertical connectors, as well as the mean position and the standard deviation of the position in the X- and Y-axis directions of the connectors' extremity.

The cloud of points reveals that much larger displacements in the X-axis direction are observed at a distance from the wall centre (i.e. when Y ranges from -2 to -4 m. This is also the place where larger variability in displacement with impact conditions is observed. Also, the displacement component along the Y-axis direction is much smaller at the wall centre (Y=0m) than that 2.5m aside. These differences in wall displacement according to the impact location along the wall longitudinal axis are attributed to the zig-zag conformation of the wall. Basically, the interconnections between the blocks favour significant displacement of blocks at a distance from the impact location, which number depends on the impact location. Basically, if the number of blocks experiencing displacement is small for a given impact location, then the displacement of the impacted block is large, and vice-versa.

The variability in wall response with the impact conditions is also revealed by the variation in $R_{f/p}$, whose value typically ranged from approximately 0.4 to 3.8 over the 300 simulations (Fig. 7). This figure suggests a trend concerning the impact inclination angle where an increase in the impact inclination angle, α, above 0° results in an increase in the minimum value of $R_{f/p}$, meaning an increase in the relative contribution of friction over plastic strain in total energy dissipation. To a much lesser extent, the minimum value of $R_{f/p}$ seems to slightly vary with y and β.

Apart from α, no clear trend for the influence of the parameters can be directly derived from this simple figure.

The Sobol indices are much more informative and confirm the influence of α. The method proposed by Sobol (1993) consists in decomposing the variance of the output parameters as the sum of the contributions of the different input parameters including the possible interaction between input parameters. Each contribution is characterised by the ratios of the partial variance to the total variance, called Sobol sensitivity indices. As for the impact location, $R_{f/p}$ is particularly dependant on the position along the wall longitudinal axis, y, but not on that along the vertical axis, z. In a rather counterintuitive manner, the projectile translational velocity, v, appears to have a very small influence. The influence of the deviation, β, appears significant.

It is worth mentioning that there is a strong dependence between these parameters as confirmed by the fact that the sum of the six Sobol indices significantly exceeds 1.0. This means that the dependence of $R_{f/p}$ on one specific parameter, is influenced by the value of another parameter. For example, the influence of the deviation angle, β, depends on the impact location along the wall longitudinal axis, y, due to the wall zig-zag conformation. The interrelationship also explains why no strong trend can be observed in Figure 7 , at the exception as for α.

The distribution of $R_{f/p}$ was computed from the 300 simulation results complemented with a refined distribution obtained from a specifically developed PCE-based meta-model (Fig. 9, top). This figure shows that the main dissipative mechanism is the plastic strain in the block (globally, $R_{f/p} < 1$). Energy dissipation by friction appears to be negligible in some impact cases with $R_{f/p}$ values much less than 0.5. On the contrary, the amount of energy dissipated by friction is more than twice that dissipated by plastic strain in other impact situations. Comparison of this distribution with the value of dissipation ratio $R_{f/p}$ obtained for the two impact tests against which the model was calibrated (0.56 and 0.55) reveals that these test conditions favoured even more dissipation by plastic strain.

Considering separately cases where the impact energy is higher or lower than 500kJ leads to the same general conclusion (Fig. 9, bottom) meaning that the relative contribution of friction with respect to plastic strain in energy dissipation is the same whether the projectile velocity is high or low (because its mass was not varied). This comment is in line with the previous one on the influence of the projectile velocity on $R_{f/p}$.

Overall, the prevailing dissipative mechanism appears to be block plastic strain, but there exists a strong dependence on the impact conditions. Besides, normal-to-the-wall impacts result in $R_{f/p}$ values which do not reflect the average wall dissipative capacities, meaning that the precise assessment of its on-site response in terms of energy dissipation should not be extrapolated from results from such tests.

5.3 Interpretation

The results presented in Figures 7, 8 and 9 convey information of great value for understanding the structure response and assessing its dissipative capacities.

The displacement of the structure and the amount of energy it dissipates by plastic strain and friction depends on the energy that is transferred to the wall during the impact. This amount of energy, referred to as "imparted energy", E_{impart}, is considered equal to the variation in projectile total energy during the impact:

$$E_{impart} = \Delta\big(P_{proj} + K_{proj}\big) \tag{12}$$

The ratio between the imparted energy, E_{impart}, and the projectile kinetic energy at impact, $K_{proj}(t_0)$, ranges from approximately 0.25 to 1 depending on the impact conditions (Fig. 10, top). The variability in this ratio is governed by the inclination angle, α, and other parameters having negligible influence (Fig. 10, bottom). Lower values of this ratio are observed for high and low values of α (Fig. 10, top). This is attributed to the fact that a deviation in trajectory with respect to the normal of the impacted concrete block favours projectile deviation, resulting in a higher projectile rebound velocity and a lower E_{impart}. Such non-normal impacts also result in lower impact forces on the impacted concrete block, and thus less plastic damage to this block. These two comments are thought to explain the trend for the influence of α as well as for the influence of β on the minimum value of $R_{f/p}$ where a lower contribution of plastic strain is observed when the deviation of the projectile trajectory with respect to the normal to the impacted block is higher.

The virtually negligible influence of the translational velocity on the relative contribution between the two dissipative mechanisms, i.e. $R_{f/p}$ ratio, (Fig. 8) is partially attributed to the Gaussian distribution considered for this parameter which results in less frequent extreme velocity values in the set of impact conditions.

The $R_{f/p}$ ratio refers to the relative contribution of friction over plastic strain in energy dissipation but does not indicate the amount of energy that is dissipated in the wall. For this reason, evaluating the criticality of an impact in terms of displacement or damage requires also accounting for the amount of energy the wall dissipates during impact, which equals E_{impart}. In other words, a very low, resp. high, value of $R_{f/p}$ will lead to high damage, resp. displacement, only if the energy that is transferred to the wall during impact is high.

The structure efficiency analysis conducted combining $R_{f/p}$ with the imparted energy, E_{impart}, reveals a certain correlation between the two variables, where lower $R_{f/p}$ values are globally associated with impact conditions where E_{impart} is high, and, inversely, higher $R_{f/p}$ values correspond to lower values of E_{impart} (see Fig. 11). Impact situations where the projectile incident trajectory is horizontal, with α values close to 0°, are globally associated with higher E_{impart} values. On the contrary, extreme values of inclination ($\alpha <$ -45° or $\alpha >$ 45° approx.) lead to E_{impart} values less than 400kJ. This figure confirms that downward projectile trajectories (positive α values) tend to favour dissipation by friction, with $R_{f/p}$ values most often higher than 1 while upward projectile trajectories tend to favour dissipation by plastic strain, with $R_{f/p}$ values most often lower than 1. These comments are in line with the previous comments on the influence of α on the structure response.

While Figure 9 revealed that the number of impact conditions where dissipation by plastic strain was statistically dominating, Figure 11 shows that the structure response over this wide range of impact conditions is such that conditions where plastic strain dominates are associated with a large amount of energy dissipated by the structure. This leads to the conclusion that the probability of having large damage to concrete blocks is high with this zig-zag conformation wall.

6 Perspectives

In this work, the dissipative capacities of the structure were addressed by varying the parameters describing the impact conditions over realistic ranges and considering realistic but rather arbitrary distributions (see Table 1). Important findings derived from figures 9 and 11, in particular, are related to these ranges and distributions.

Nevertheless, these ranges and distributions are not fully representative of that derived from rockfall trajectory simulations on real sites. In a very similar context, Lambert et al (2021) have shown that the efficiency of flexible barriers in arresting rock blocks was extremely sensitive to the distributions of the impact condition parameters, even when the barrier was designed for the concerned site.

In addition, there exists some couplings between the parameters. In particular, upward incident trajectories relate to cases where the rock block bounces in the ditch uphill of the structure before impacting it. This bounce induces energy dissipation and, for this reason, the rock block translational velocity at impact on the structure is, on the average, much less than in the case of a block directly impacting the structure with a downward trajectory. These couplings exist and are site-specific but were not accounted for when sampling the 300 sets of input parameters.

These comments suggest that the structure dissipative capacity for a given site may statistically differ from that derived from the results presented herein. The mean value of 0.8 approx. for $R_{f/p}$ is not relevant for all sites. As a consequence, the wall effective dissipative capacities for a given site should rather be quantified considering the site-specific range of impact conditions which are obtained from rockfall trajectory simulations (Lambert et al, 2021).

For the considered wall, with a zig-zag conformation, the main dissipative mechanism was associated with concrete block damage. The dissipation ratio $R_{f/p}$ had an average value of 0.8, meaning that 55% of energy dissipation was due to plastic strain. Depending on the impact conditions, the contribution of plastic strain on total energy dissipation varied between 20% and 70% approx., corresponding to the highest and lowest observed $R_{f/p}$ values respectively (3.8 and 0.4). Taking advantage of the versatility of this structure type, its design could be improved, in particular considering other conformations. This design optimisation could be based on the $R_{f/p}$ ratio following different strategies in terms of functional requirements. One optimisation strategy could consist of preventing both large damage to the concrete blocks and large wall displacement whatever the impact conditions. In such an approach, the optimum design would be such that the ratio $R_{f/p}$ remains within a limited range such that friction and plastic strain rather equally contribute to energy dissipation in any case. Another strategy could consist of designing a wall favouring displacement, to prevent damage to concrete blocks, as damage to concrete blocks requires work for their replacement. In such a purpose, the wall pattern could be modified so that the probability of having a low $R_{f/p}$ value is lower than that for the zig-zag pattern. Whatever the goal of the design optimisation, the value of the ratio should always be complemented with the imparted energy, E_{impart}, as large damage or displacement requires that the amount of energy transferred to the wall is also sufficiently high.

From a methodological point of view, conducting such design improvements would require performing a large number of NSCD simulations (typically 300) for each design, from which a meta-model would be developed for supplying the $R_{f/p}$ values.

7 Conclusions

The efficiency of protection structures exposed to impact, among which passive rockfall protection structures, largely depends on their energy dissipative capacities. This work addressed the impact response of such structures in terms of energy dissipation, and highlighted the potential of an accurate energy dissipation quantification. It was based on the example of a rockfall protection wall made of interconnected concrete blocks for which a numerical model developed under the NSCD framework and calibrated from real-scale impact experiments was available. Under the assumption that the concrete block and dissipation mechanisms are reasonably well modelled with respect to the addressed topic, the conclusions are:

- the method proposed to derive the energy dissipated by both friction and plastic strain from NSCD simulation results was demonstrated to ensure energy conservation in the system throughout the simulation, whose feature results from the fact that the numerical scheme respects the discrete energy/work balance.
- for the NSCD model of this structure to provide a reliable quantification of the dissipative energy terms, the calibration of its five parameters should be based on at least two measures obtained from real-scale impact experiments.
- the ratio between the cumulative contribution to energy dissipation of friction and plastic strain, $R_{f/p}$, is proposed as a descriptor of the whole structure impact response with time and to assess its energy dissipative capacities.
- the combination of the $R_{f/p}$ value with the energy imparted to this wall, E_{impart}, revealed that damage to concrete blocks was the dominating dissipative mechanism when considering a wide range of realistic impact conditions.
- the response of this wall, in particular in terms of $R_{f/p}$ value, is primarily governed by the incident projectile trajectory inclination angle, which also governs E_{impart}.

Focus was placed on a particular type of passive protection structure but the general principle of addressing its response based on energy dissipation quantification could be applied to any type of structure exposed to impact in which energy is dissipated by two mechanisms mainly, and in particular rockfall protective structures such as flexible barriers or rockfall protection embankments.

As a perspective, the general approach will be considered for improving the design of articulated walls when considering site-specific impact conditions, for example in view of optimising the wall conformation based on the $R_{f/p}$ ratio.

References

Acary V, Collins-Craft NA (2024) On the Moreau–Jean scheme with the Frémond impact law. Energy conservation and dissipation properties for elastodynamics with contact impact and friction, URL https://inria.hal.science/hal-04230941v2, working paper or preprint

Acary V, Perignon F (2007) Siconos: A Software Platform for Modeling, Simulation, Analysis and Control of Nonsmooth Dynamical Systems. SIMULATION NEWS EUROPE, ArgeSIM/ASIM 17(3/4):19–26. URL //hal.inria.fr/inria-00522740/document

Acary V, Brémond M, Huber O (2018) Advanced Topics in Nonsmooth Dynamics., Acary, V. and Brüls. O. and Leine, R. (eds). Springer Verlag, chap On solving frictional contact problems: formulations and comparisons of numerical methods., p 375–457

Acary V, Bonnefon O, Brémond M, et al (2019) An introduction to Siconos. Technical report

Bourrier F, Berger F, Tardif P, et al (2012) Rockfall rebound: comparison of detailed field experiments and alternative modelling approaches. Earth Surface Processes and Landforms 37(6):656–665. https://doi.org/10.1002/esp.3202

Bourrier F, Baroth J, Lambert S (2016) Accounting for the variability of rock detachment conditions in designing rockfall protection structures. Natural Hazards https://doi.org/10.1007/s11069-015-2084-0

Breugnot A, Lambert S, Villard P, et al (2016) A discrete/continuous coupled approach for modeling impacts on cellular geostructures. Rock Mechanics and Rock Engineering https://doi.org/10.1007/s00603-015-0886-8.

Castanon-Jano L, Blanco-Fernandez E, Castro-Fresno D (2019) Design of a new energy dissipating device and verification for use in rockfall protection barriers. Engineering Structures 199:109633. https://doi.org/10.1016/j.engstruct.2019.109633

Dhankal S, Bhandary NP, Yatabe R, et al (2012) Numerical and analytical investigation towards performance enhancement of a newly developed rockfall protective cable-net structure. Natural Hazards and Earth System Sciences 12(4):1135–1149. https://doi.org/10.5194/nhess-12-1135-2012

Di Giacinto D, Grassia L, Capriello G, et al (2020) A novel steel damping system for rockfall protection galleries. Journal of Constructional Steel Research 175:106360. https://doi.org/10.1016/j.jcsr.2020.106360

Douthe C, Girardon C, Boulaud R (2022) Sensitivity analysis of the global response of flexible rockfall barriers. Geosciences 12(2). https://doi.org/10.3390/geosciences12020075

Duan S, Yu H, Xu B (2023) Numerical simulation of a rockfall impacting a gravel cushion with varying initial angular velocity and particle sizes. Granular Matter 33(25). https://doi.org/10.1007/s10035-023-01320-3

Dubois F, Acary V, Jean M (2018) The Contact Dynamics method: A nonsmooth story . Comptes Rendus Mécanique 346(3):247–262. https://doi.org/10.1016/j.crme.2017.12.009

EOTA (2018) Ead 340059-00-0106: Falling rock protections kits

Frémond M (2017) Collisions in mechanics. Annals of Solid and Structural Mechanics 9:29–56

Frémond M (2002) Non-Smooth Thermo-mechanics. Springer-Verlag, Berlin-Heidelberg

Furet A, Lambert S, Villard P, et al (2022) Experimental and numerical impact responses of an innovative rockfall protection structure made of articulated concrete blocks . Rock Mechanics and Rock Engineering https://doi.org/doi.org/10.1007/s00603-022-02957-x

Gupta R, Bourrier F, Acary V, et al (2023) Bayesian interface based calibration of a novel rockfall protection structure modelled in the non-smooth contact dynamics framework. Engineering structures 297. https://doi.org/0.1016/j.engstruct.2023.116936

Gupta R, Bourrier F, Lambert S (2024) Bayesian inference based inverse analysis of the impact response of a rockfall protection structure: Application towards warning and survey. Engineering Structures https://doi.org/10.1016/j.engstruct.2024.118800

Jean M (1999) The non smooth contact dynamics method. Computer Methods in Applied Mechanics and Engineering 177:235–257. Special issue on computational modeling of contact and friction, J.A.C. Martins and A. Klarbring, editors

Jean M, Moreau JJ (1987) Dynamics in the presence of unilateral contacts and dry friction: a numerical approach. In: Del Pietro G, Maceri F (eds) Unilateral problems in structural analysis. II. CISM 304, Spinger Verlag, p 151–196

Korini O, Bost M, Rajot JP, et al (2021) The influence of geosynthetics design on the behavior of reinforced soil embankments subjected to rockfall impacts. Engineering Geology

Lambert S, Bourrier F (2013) Design of rockfall protection embankments: A review. Engineering Geology 154:77–88

Lambert S, Bourrier F, Gotteland P, et al (2019) An experimental investigation of the response of slender protective structures to rockfall impacts. Canadian geotechnical journal https://doi.org/10.1139/cgj-2019-0147

Lambert S, Toe D, Mentani A, et al (2021) A Meta-Model-Based Procedure for Quantifying the On-Site Efficiency of Rockfall Barriers. Rock Mechanics and Rock Engineering 54(2):487–500. https://doi.org/10.1007/s00603-020-02298-7

Lataniotis C, Marelli S, Sudret B (2015) Uqlab user manual – the input module. Tech. rep., Chair of Risk, Safety & Uncertainty Quantification, ETH Zurich, report UQLab-V0.9-102

Liang G, Junfa Z, Hanlin L (2022) Impact resistance of unequal diameter double u-shaped metal energy dissipation bearing. Structures 41:404–418. https://doi.org/10.1016/j.istruc.2022.05.019

Liu C, Tian S, Xu C, et al (2018) Study on mechanical properties and dissipation capacity of ring net in passive rockfall barriers. Natural hazards and earth systems science https://doi.org/10.5194/nhess-2018-76

Maheshwari S, Bhowmik R, Cuomo S (2024) Impact performance of unreinforced and geogrid-reinforced rockfall protection embankment. Geosynthetics International https://doi.org/10.1680/jgein.23.00159

Marchelli M, Deangeli C (2022) Towards a codified design procedure for rockfall reinforced earth embankments. Geoingegneria e attività estrattiva pp 50–59. https://doi.org/10.19199/2022.165.1121-9041.0502

Mentani A, Govoni L, Gottardi G, et al (2016) A new approach to evaluate the effectiveness of rockfall barriers. Procedia Engineering 158:398–403. https://doi.org/10.1016/j.proeng.2016.08.462, vI Italian Conference of Researchers in Geotechnical Engineering, CNRIG2016 - Geotechnical Engineering in Multidisciplinary Research: from Microscale to Regional Scale, 22-23 September 2016, Bologna (Italy)

Ng CW, Zhang D, Choi CE, et al (2023) Analysis of steel baffle installed on footing with dowels for resisting boulder impact. Engineering Geology 312:106956. https://doi.org/10.1016/j.enggeo.2022.106956

Noël F, Nordang SF, Jaboyedoff M, et al (2023) Comparing flow-r, rockyfor3d and ramms to rockfalls from the mel de la niva mountain: A benchmarking exercise. Geosciences 13(7). https://doi.org/10.3390/geosciences13070200

Previtali M, Ciantia MO, Spadea S, et al (2021) Multiscale modelling of dynamic impact on highly deformable compound rockfall fence nets. Proceedings of the Institution of Civil Engineers - Geotechnical Engineering 174(5):498–511. https://doi.org/10.1680/jgeen.21.00108

Previtali M, Ciantia MO, Spadea S, et al (2023) Assessing rockfall barrier performance through block propagation codes and meta-models. In: Barla M, Di Donna A, Sterpi D, et al (eds) Challenges and Innovations in Geomechanics. Springer International Publishing, Cham, pp 291–298

Qi X, Zhao L, Hao C, et al (2022) Numerical simulation of dynamic responses of semi-rigid rockfall protection barriers subjected to impact loading at different positions. Bulletin of Engineering Geology and the Environment 81. https://doi.org/10.1007/s10064-022-02870-1

Ronco C, Oggeri C, Peila D (2009) Design of reinforced ground embankments used for rockfall protection. Natural Hazards and Earth System Science https://doi.org/10.5194/nhess-9-1189-2009

Sobol IM (1993) A screening design for factorial experiments with interactions. Mathematical and Computer Modelling 1:407–414

Toe D, Mentani A, Govoni L, et al (2018) Introducing meta-models for a more efficient hazard mitigation strategy with rockfall protection barriers. Rock Mechanics and Rock Engineering

Volkwein A, Schellenberg K, Labiouse V, et al (2011) Rockfall characterisation and structural protection – a review. Natural Hazards and Earth System Sciences 11(9):2617–2651. https://doi.org/10.5194/nhess-11-2617-2011

Xu H, Gentilini C, Yu Z, et al (2018) An energy allocation based design approach for flexible rockfall protection barriers. Engineering Structures 173:831–852. https://doi.org/10.1016/j.engstruct.2018.07.018

Yan S, Wang Y, Wang D, et al (2022) Application of eps geofoam in rockfall galleries: Insights from large-scale experiments and fdem simulations. Geotextiles and Geomembranes 50(4):677–693. https://doi.org/10.1016/j.geotexmem.2022.03.009

Yang G, Qiao F, Lu F, et al (2024) Discrete element modelling of rock-filled gabions under successive boulder impacts. Computers and geotechnics

Yu Z, Zhao L, Liu Y, et al (2019) Studies on flexible rockfall barriers for failure modes, mechanisms and design strategies: a case study of western china. Landslides 16:347–362. https://doi.org/10.1007/s10346-018-1093-y

Zhao L, Zhang LJ, Yu ZX, et al (2021) Energy dissipating modes and design recommendation of h-shaped steel baffles subjected to boulder impact. Advanced Steel Construction 17:349–355. https://doi.org/https://10.18057/IJASC.2021.17.4.3

A Computation scheme

In our context of 3D rigid bodies, the equation of motion with contact and Coulomb friction is given by:

$$\left\{\begin{array}{l} \dot{q} = T(q)v,\\ M\dot{v} = F(t,q,v) + G^\top(q)r,\\ \left.\begin{array}{ll} u^\alpha = G^\alpha(q)v & \\ r^\alpha = 0, & \text{if } g_{\mathrm{N}}^\alpha(q) > 0,\\ K^{\alpha,*} \ni \widehat{u}^\alpha \perp r^\alpha \in K^\alpha, & \text{if } g_{\mathrm{N}}^\alpha(q) = 0,\\ u_{\mathrm{N}}^{\alpha,+} = -e^\alpha u_{\mathrm{N}}^{\alpha,-}, & \text{if } g_{\mathrm{N}}^\alpha(q) = 0 \text{ and } u_{\mathrm{N}}^{\alpha,-} \leq 0 \end{array}\right\} \alpha \in \mathcal{I}, \end{array}\right.$$

The vector q is the configuration vector which combines the position of the centre of mass and the parameterisation of the rotation with quaternions for each body. The generalised velocity vector v contains the centre of mass velocities and the angular velocities expressed in the body frame. The $x \perp y$ symbol means that $y^\top x = 0$. The matrix $T(q)$ relates the time derivative of q to v. $\mathcal{I}$ is the set of potential contacts and $g_{\mathrm{N}}^\alpha(q)$ is the gap function associated to the distance between bodies potentially in contact. The matrix M is the mass matrix, the vector F is the force vector that collects the external applied forces and the gyroscopic effects. For the contact point $\alpha \in \mathcal{I}$, the matrix $G^\alpha(q)$ is the contact configuration matrix, which expresses the local relative contact velocity u in terms of the generalised velocities v. The matrix $G(q)$ collects the matrices $G^\alpha(q)$ for $\alpha \in \mathcal{I}$.

The reaction forces r^α and the velocities u^α are decomposed into their normal and tangent parts, denoted $r_{\mathrm{N}}, r_{\mathrm{T}}$ and u_{N}, u_{T}, respectively.

Using the modified relative contact velocity $\widehat{u}^\alpha$, such that $\widehat{u}^\alpha_{\mathrm{N}} = u^\alpha_{\mathrm{N}} + \mu^\alpha \|u^\alpha_{\mathrm{T}}\|$, $\widehat{u}^\alpha_{\mathrm{T}} = u^\alpha_{\mathrm{T}}$, the Coulomb friction with unilateral contact is expressed as (see Acary et al (2018) for details) :

$$K^{\alpha,*} \ni \widehat{u}^\alpha \perp r^\alpha \in K^\alpha, \tag{13}$$

The cone $K = \{r \in I\!R^3, ||r_{\mathrm{T}}|| \leq \mu r_{\mathrm{N}}\}$ is the usual Coulomb friction cone and $K^* = \{z \in I\!R^3 \mid z^T x \geq 0 \text{ for all } x \in K\}$ its dual.

The formulation is completely equivalent to the standard Coulomb friction model with contact as shown in (Acary and Collins-Craft, 2024). The relation $u^{\alpha,+}_{\mathrm{N}} = -e^\alpha u^{\alpha,-}_{\mathrm{N}}$ is the Newton impact law for the contact α.

In order to take into account the impact phenomenon in case of a jump in velocity, in a way that is consistent with the energy dissipation, the contact law is written with the help of Frémond's approach (Frémond, 2017; Frémond, 2002) as

$$K^{\alpha,*} \ni \begin{bmatrix} \bar{u}_{\mathrm{N}} + \frac{1}{2} e u^-_{\mathrm{N}} + \mu^\alpha \|\bar{u}^\alpha_{\mathrm{T}}\| \\ \bar{u}_{\mathrm{T}} \end{bmatrix} \perp p^\alpha \in K^\alpha, \tag{14}$$

where $\bar{u} = \frac{1}{2}(u^{\alpha,+} + u^{\alpha,-})$ is the average of the pre- and post-impact velocities, and p^α the contact impulse.

With the Frémond's approach, the Moreau–Jean scheme (with $\theta = 1/2$) for the system, for a time discretization $t_0 < \ldots < t_k < t_{k+1} < \ldots < t_n$ with a time step

$h = t_{k+1} - t_k$, is adapted as follows

$$\begin{cases} q_{k+1} = q_k + hT(q_{k+1/2})v_{k+1/2} \\ M(v_{k+1} - v_k) - hF_{k+1/2} = G^\top(q_k)p_{k+1}, \\ u_{k+1/2} = G(q_k)v_{k+1/2}, \\ \left.\begin{array}{l} p^\alpha_{k+1} = 0, \end{array}\right\} \alpha \notin \mathcal{I}_k \\ \left.\begin{array}{l} K^{\alpha,*} \ni \widetilde{u}^\alpha_{k+1/2} \ \perp p^\alpha_{k+1} \in K^\alpha \end{array}\right\} \alpha \in \mathcal{I}_k. \end{cases} \tag{15}$$

with

$$\widetilde{u}_{k+1/2} = \begin{bmatrix} u_{\mathrm{N},k+1/2} + \frac{1}{2}(e-1)u_{\mathrm{N},k} + \mu^\alpha \|u^\alpha_{\mathrm{T},k+1/2}\| \\ \bar{u}_{\mathrm{T},k+1/2} \end{bmatrix} \tag{16}$$

to be consistent with Equation (14). The standard notation $x_{k+1/2} = 1/2(x_k + x_{k+1})$ is used. The set $\mathcal{I}_k$ is the set of contacts activated at the velocity level:

$$\mathcal{I}_k = \{\alpha \in I \mid g^\alpha_{\mathrm{N},k} + \frac{1}{2}u^\alpha_{\mathrm{N},k} \leq 0, \text{ and } u^\alpha_{\mathrm{N},k} \leq 0\} \tag{17}$$

Table 1 Parameters value of the different models employed in this study

Model	d_z (cm)	v_p (cm)	μ_{cc} (-)	μ_{cs} (-)	e (-)
Reference	7.3	6.7	0.313	0.310	0.221
CS1	9.4	7.1	0.392	0.307	0.135
CS2	9.8	3.7	0.277	0.417	0.018
CS3	6.0	7.6	0.289	0.427	0.284
CS4	9.0	5.0	0.309	0.344	0.296
CS5	7.0	8.7	0.251	0.315	0.291
CS6	6.9	9.9	0.542	0.301	0.288
CS7	6.7	9.0	0.253	0.322	0.296
CS8	8.9	3.9	0.389	0.305	0.107
CS9	5.1	9.7	0.257	0.308	0.209

Table 2 Alternative calibration strategies and origin of the calibration data.

Id.	Considered point(s)	Considered time(s)	Considered energy(ies)	Numb. of calib. data
CS1	Base	Rest	520kJ	1
CS2	Top	Rest	520kJ	1
CS3	D	Rest	520kJ	1
CS4	Top	Max.	520kJ	1
CS5	D	Rest	1020kJ	1
CS6	D	Init. + max. + rest	520kJ	3
CS7	D	Rest	520 + 1020kJ	2
CS8	Base + D	Rest	520kJ	2
CS9	Base + D	Rest	1020kJ	2

Table 3 Model parameters with their respective ranges

Param.	Range	Distribution	Unit
Translational velocity (v)	10 - 25	Gaussian	m/s
Rotational velocity (Ω)	0.0 - 5.6	Uniform	rot/s
Impact pos. - along length (y)	0.0 - -3.53	Uniform	m
Impact pos. - along wall height (z)	0.55 - 2.10	Uniform	m
Impact inclination (α)	-60 - +60	Uniform	°
Impact deviation (β)	-45 - +45	Gaussian	°

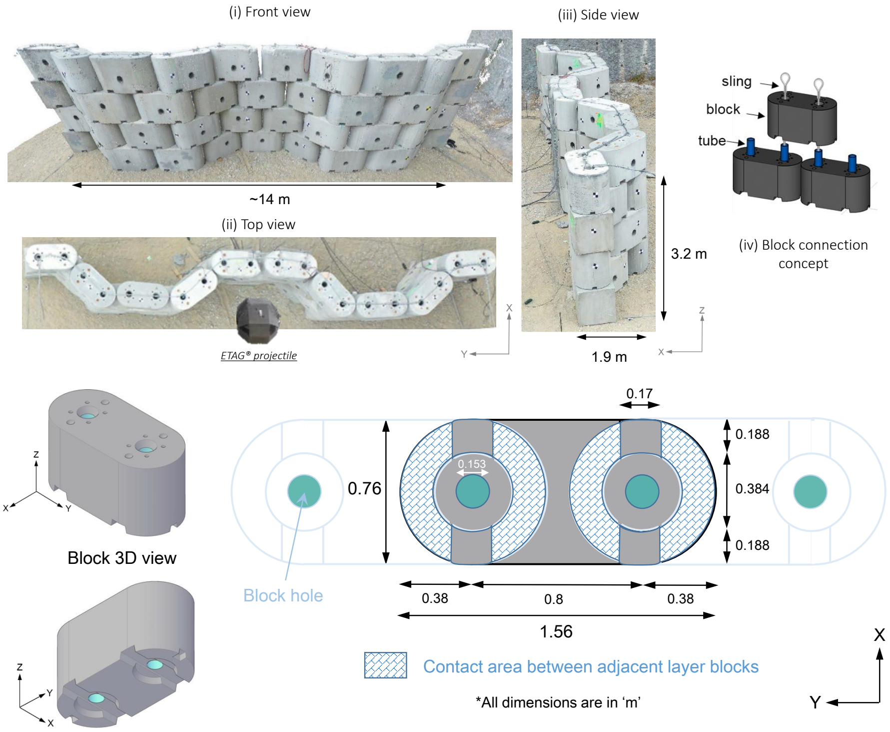

Fig. 1 (a) Experimental full-scale structure and (b) concrete block geometry and dimensions

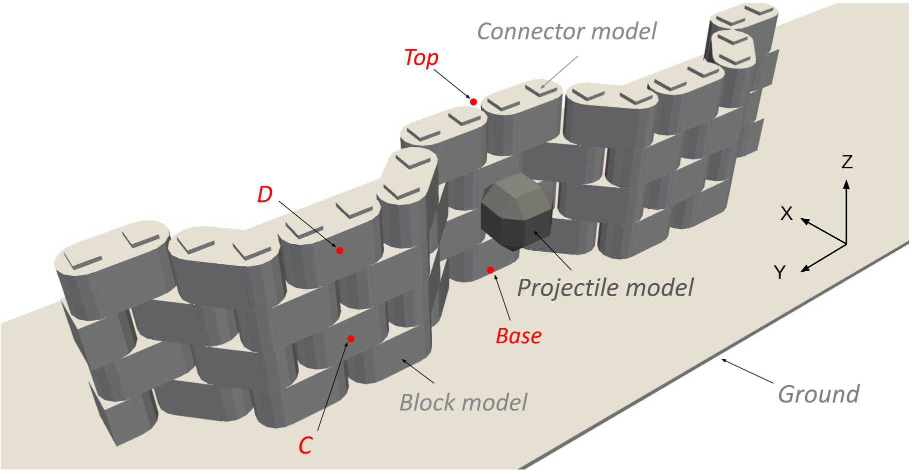

Fig. 2 The NSCD model of the articulated structure and its components, taken from (Gupta et al, 2023). Location of points where data were collected during the real-scale experiments ('Base', 'Top', 'C' and 'D').

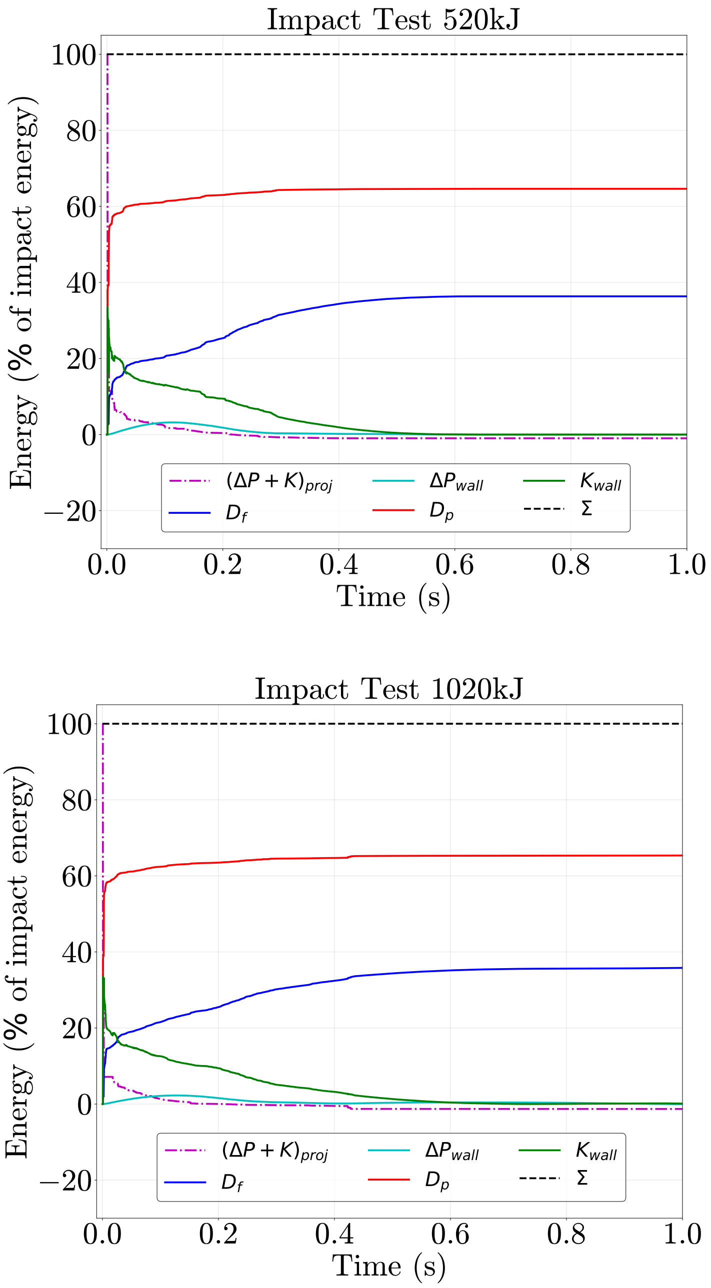

Fig. 3 Energy in the system obtained from the simulation of the structure response to 520- and 1020kJ-energy impacts.

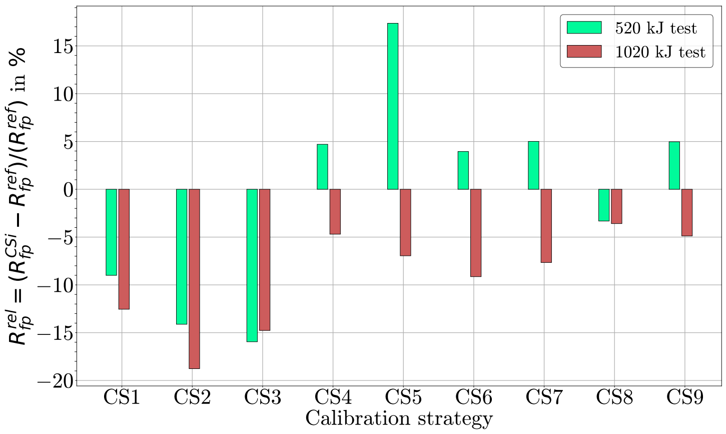

Fig. 4 Relative difference in the ratio of energy dissipated by friction to energy dissipated by plastic strain obtained with the models calibrated against the various strategies listed in Table 2 with respect to the ratio value obtained with the reference model.

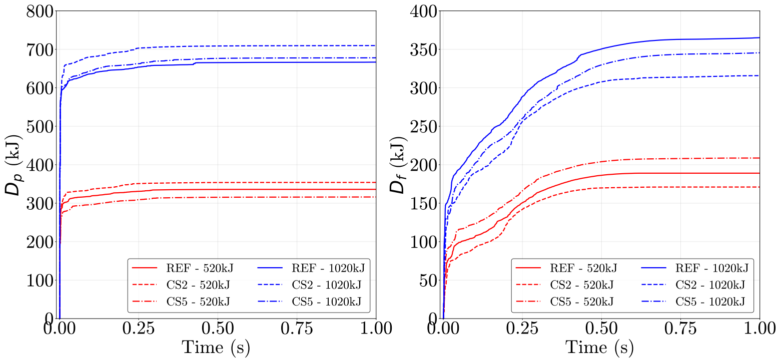

Fig. 5 Energy dissipated in the wall based on simulation results with models calibrated following strategies CS2 and CS5 compared with the reference model: energy dissipated by plastic strain, D_p (left) and energy

dissipated by friction, D_f (right).

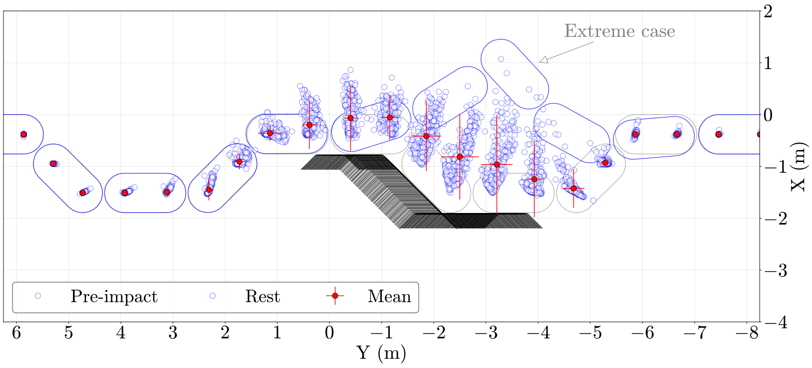

Fig. 6 Displacement at the top of the wall after impacts under different conditions. The dark area shows the range of the impact point location. Axis are defined in Figure 2.

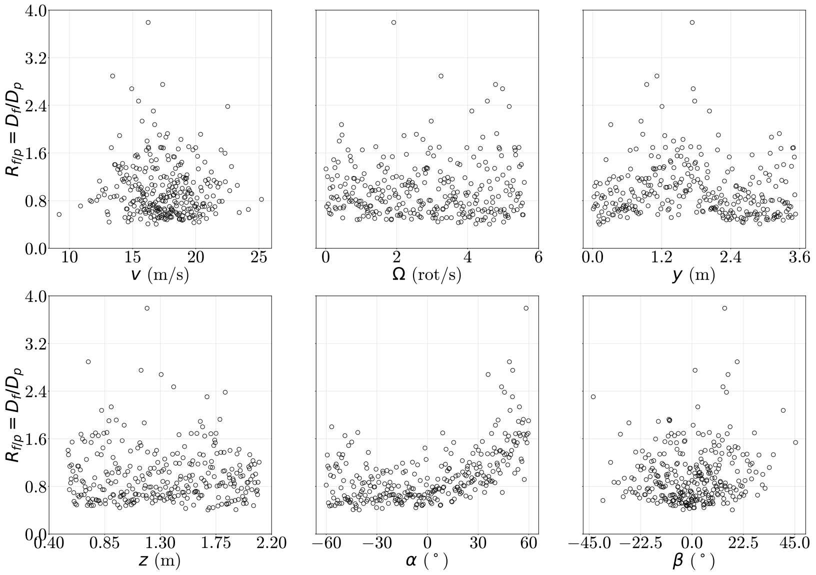

Fig. 7 Dissipation ratio ($R_{f/p}$) vs. each of the six parameters describing the impact conditions for all 300 simulations.

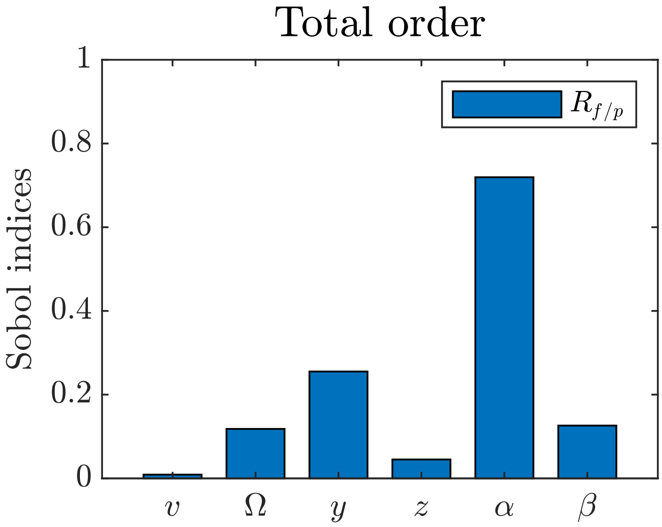

Fig. 8 Total Sobol indices for the dissipation ratio.

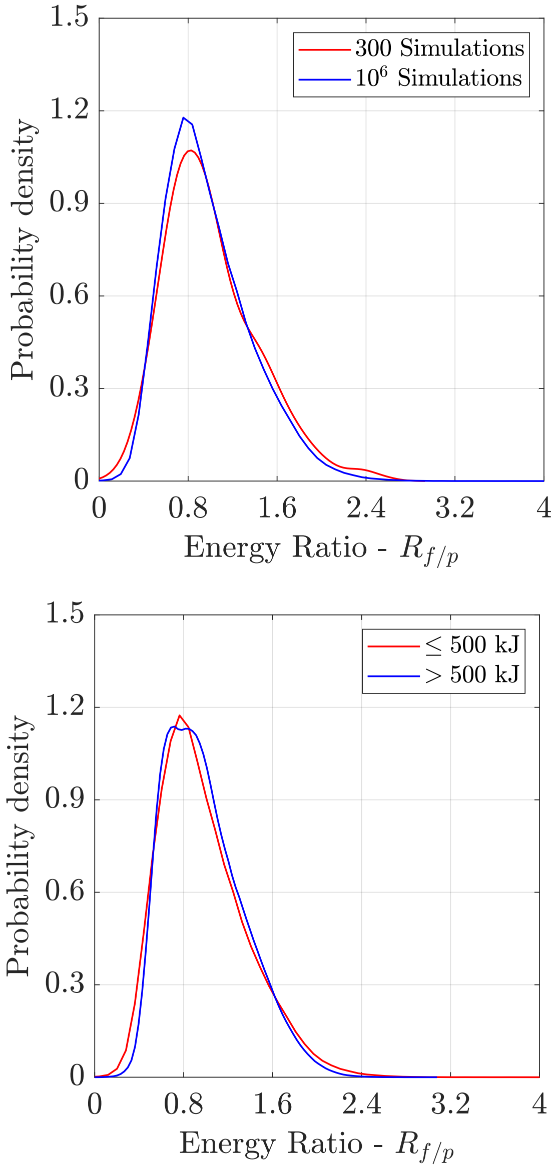

Fig. 9 Distribution of $R_{f/p}$ varying the impact conditions (top) for different numbers of simulations and (bottom) for different ranges of incident projectile kinetic energy.

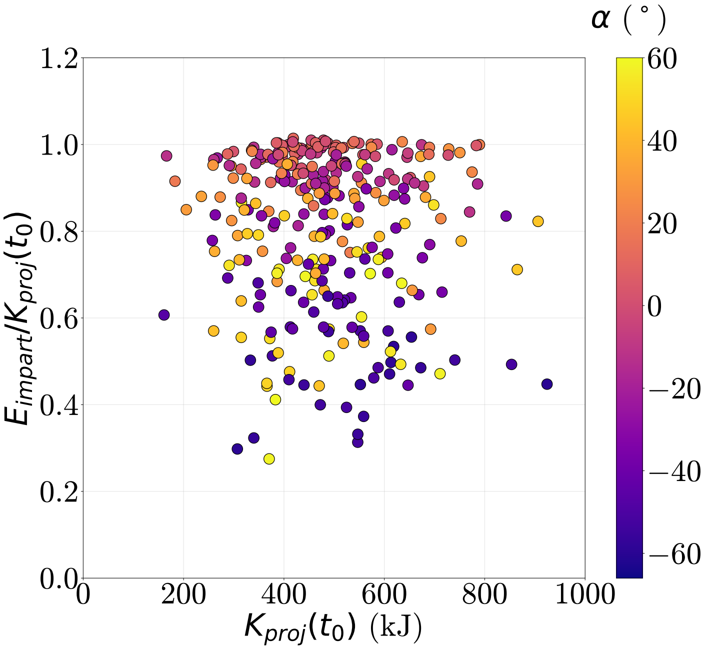

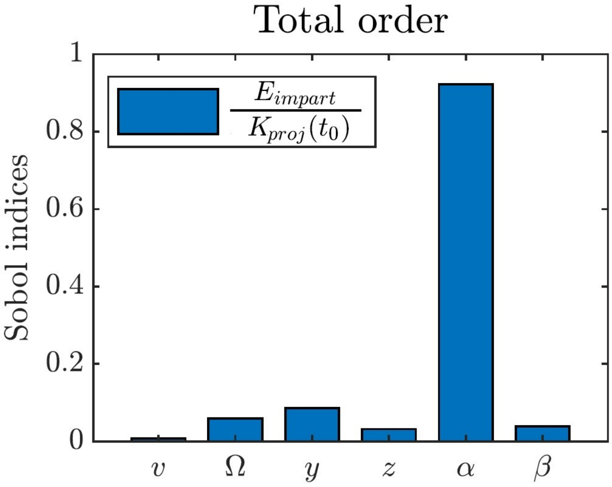

Fig. 10 Ratio of energy imparted to the wall (E_{impart}) to the projectile kinetic energy at impact (top), and the total Sobol indices of ICPs for this ratio (bottom). Computed from the 300 NSCD model simulations.

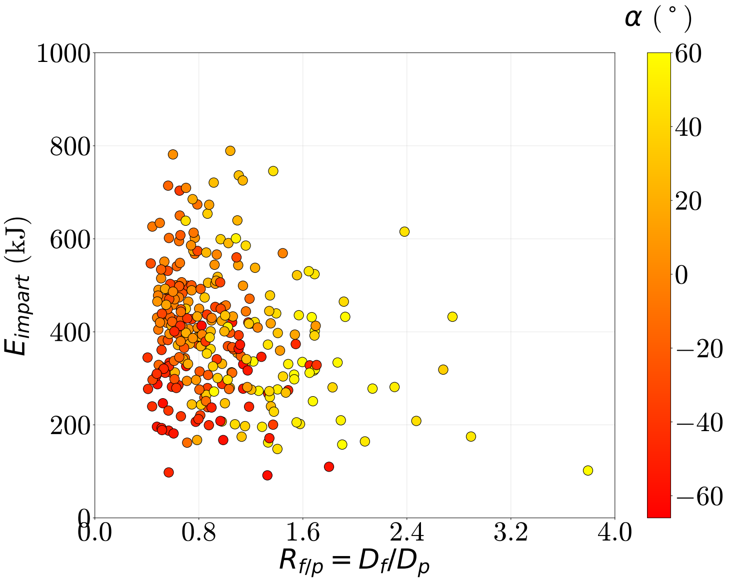

Fig. 11 Energy transferred to the wall and ratio between energy dissipated by friction and energy dissipated by plastic strain ($R_{f/p}$). Results from the set of 300 simulations varying the impact conditions.